LBL-30347

Lawrence Berkeley Laboratory
UNIVERSITY OF CALIFORNIA

Materials & Chemical Sciences Division

To be published as a chapter in **The Science of Ceramic Interfaces**, J. Nowotny, Ed,.Elsevier Science Publishers, Amsterdam, The Netherlands, 1991

The Role of Interfaces in Sintering: An Experimental Perspective

A.M. Glaeser

February 1991

U. C. Lawrence Berkeley Laboratory
Library, Berkeley

FOR REFERENCE

Not to be taken from this room

LBL-30347
Copy 1
Bldg. 50 Library.

Prepared for the U.S. Department of Energy under Contract Number DE-AC03-76SF00098

DISCLAIMER

This document was prepared as an account of work sponsored by the United States Government. While this document is believed to contain correct information, neither the United States Government nor any agency thereof, nor the Regents of the University of California, nor any of their employees, makes any warranty, express or implied, or assumes any legal responsibility for the accuracy, completeness, or usefulness of any information, apparatus, product, or process disclosed, or represents that its use would not infringe privately owned rights. Reference herein to any specific commercial product, process, or service by its trade name, trademark, manufacturer, or otherwise, does not necessarily constitute or imply its endorsement, recommendation, or favoring by the United States Government or any agency thereof, or the Regents of the University of California. The views and opinions of authors expressed herein do not necessarily state or reflect those of the United States Government or any agency thereof or the Regents of the University of California.

THE ROLE OF INTERFACES IN SINTERING: AN EXPERIMENTAL PERSPECTIVE

Andreas M. GLAESER

Department of Materials Science and Mineral Engineering, University of California, and Materials Sciences Division, Lawrence Berkeley Laboratory, Berkeley, CA 94720 USA

The path of microstructural evolution during the initial stages of sintering is extremely sensitive to the relative rates of the transport processes that promote coarsening and densification. During the later stages of sintering, grain boundary migration and the interaction of pores with migrating grain boundaries assume a major role in determining the path of microstructural evolution. One objective of this chapter is to review these aspects of microstructural evolution. A parallel objective is to discuss some new lithography-based experimental approaches to studying the coarsening-densification competion and pore-boundary interactions. These new model experiments may provide a valuable framework for improving our understanding of the thermodynamic properties and kinetic characteristics of interfaces, their sensitivity to impurities, and more generally, the role that interfaces play in the sintering of ceramics.

1. INTRODUCTION

Most ceramics are fabricated from powders that have an average particle size in the range of a few tenths to several microns. As a result, the specific surface area of the powders and of compacts formed from them is typically of the order of several m^2/g. Pore structures in well-packed compacts also have a characteristic dimension of the order of a micron or less. Multimodal packing and the use of nanosize powders drive the size scale of interest even lower. The interfacial area to volume ratio scales inversely with a characteristic dimension of the particles (*e.g.*, a particle diameter) or of the microstructure (*e.g.*, the grain size). A trend to processing with finer particle size powders will further increase the importance of (solid-vapor) surface-related phenomena in processing and sintering. The use of finer particle size powders may also increase the specific grain boundary area at a given density, and thereby increase the relative importance of solid-solid interfacial phenomena. In materials in which a liquid or glass are present, solid-liquid interfacial phenomena will assume greater importance.

Particle size, particle size distribution, and particle packing play a major role in determining the pore size, pore size distribution, pore coordination number, pore coordination number distribution, and pore spacing in the unfired compact. The geometry of the pore structure plays an important role during the initial stages of processing. For wet-processed ceramics, the pore network provides the pathway for the removal of fluids (drying).[1] During heating, the pore network provides the

The submitted manuscript has been authored by a contractor of the U.S. Government under contract No. DE-AC03-76SF00098. Accordingly, the U.S. Government retains a nonexclusive, royalty-free licens to publish or reproduce the published form of this contribution, or allow others to do so, for U.S. Government purposes.

pathway for the redistribution and removal of organic additives (*e.g.*, binders).[2,3] There are also a number of processing approaches in which the infiltration characteristics of porous media are of interest. Green *et al.* have investigated the complete and partial infiltration of porous compacts and subsequent heat treatment as a method of producing composites.[4] Hama *et al.*[5] have investigated the infiltration of porous alumina with polymer precursors in an effort to reduce the sintering temperature of alumina. Ceramic and other preforms can be infiltrated with liquid metal as a means of fabricating ceramic-metal composites.[6,7] Stinton *et al.* have explored the use of thermal-gradient and pressure-gradient assisted vapor infiltration as a means of producing SiC-SiC composites by a nonsintering route.[8]

The microstructural changes that occur during the transformation of such an as-formed powder compact to a fired or sintered body at higher temperature reflect the relative rates of coarsening and densification. The geometry of the compact plays a major role in determining the driving forces for both coarsening and densification processes. For a given geometry, the size scale will affect the local curvature differences, transport distances, and volumetric requirements to achieve a specific change in the geometry. The coupling between these topologically dictated driving forces and grain boundary, surface, and lattice diffusivities, or interfacial reaction rate constants, or both, will ultimately determine the relative fluxes associated with competing mass source-mass sink pairs, and thus, will determine the dominant transport mechanism. Scaling law arguments[9] indicate that as the particle size is decreased, the relative importance of surface and grain boundary diffusion will increase. As a result, fundamental understanding of the thermodynamic properties and kinetic characteristics of solid-vapor and solid-solid interfaces and their impact on microstructural evolution during sintering will be increasingly necessary.

Theoretical modelling provides one route to improving our understanding of microstructural evolution during sintering. To make modelling tractable, the system is often simplified – a single transport process is assumed to dominate microstructural evolution, the properties of the material are assumed to be isotropic, a simple particle or grain geometry is assumed. Real systems are generally more complex – multiple processes interact and compete, the materials are anisotropic, and the geometries differ from those that are assumed.

This disparity between model and real microstructures can complicate the interpretation of experiments intended to test a particular model. Because it can be difficult to design experiments that match the conditions that are assumed in the modelling, the origin of differences between theory and experiment can be difficult to pinpoint. Is there is a fundamental error in the modelling, or alternatively, are concurrent processes, manifestations of anisotropy, or departures from the

assumed geometry responsible? Being able to distinguish between the two is clearly desirable. If the model is fundamentally incorrect, a completely new modelling approach may be required. If a correction term is missing or the geometry is sufficiently different from that assumed to matter, modification of an otherwise sound model is justified.

An understanding of microstructural development within powder compacts is a goal. Studies utilizing well-characterized powder compacts can have great value and are needed. However, experiments on real compacts are not necessarily adequate to test all theoretical models critically. There are phenomena of interest that are better studied using experimental methods that offer greater control over the microstructure, crystallography, and chemistry than experiments utilizing powder compacts provide. Specifically, an experimental method that provides control over the pore, flaw, or second-phase geometry, and which in some cases makes it possible to alter the relative contributions of coarsening and densification processes, has the potential to further our understanding of both the thermodynamics and kinetics of microstructural evolution, and provide a powerful supplement to more conventional experimental approaches.

Our recent experimental work has focussed on applying lithography to the study of microstructural evolution, both during sintering, and during subsequent high-temperature use. We have developed a set of model experiments that closely simulate the defect geometries that have been theoretically modelled. These model experiments provide tools for the study of: pore coarsening, pore elimination, anisotropy of grain growth, pore-boundary interactions during sintering, and high temperature crack healing.

This paper has two primary objectives. These are: 1) to briefly review the current status of models and experiments addressing the competition between coarsening and densification, grain boundary migration, and pore-boundary interactions, and 2) to describe new lithography-based experimental approaches to studying these aspects of microstructural evolution.

2. THE COARSENING-DENSIFICATION COMPETITION

2.1 MODELLING

Modelling of microstructural evolution can focus on specific processes such as neck growth, or can approach the topic from a more general perspective, and focus on the competition between processes that lead to coarsening (the reduction of surface or grain boundary area at constant density), and those that lead to densification. This latter approach was pioneered by Yan, Cannon and Chowdhry (as reported in Yan[10]). More recent modelling work by Carter and Cannon[11,12] has emphasized microstructural instabilities within a linear array of particles. The

results have important implications regarding localized desintering of compacts and damage generation during sintering. The objective of this section is to summarize the results of these models, and subsequently, to indicate how experiments utilizing lithography can provide some of the basic information required to apply these models to real systems.

Grain Size-Density Maps and Ratio Control

During the early stages of sintering, surface diffusion and evaporation-condensation can contribute to particle coarsening and interparticle neck growth without densification. Lattice diffusion and grain boundary diffusion lead to neck growth but also produce particle-particle approach. Thus, the relative rates of mass transport by surface diffusion, evaporation-condensation, lattice diffusion and grain boundary diffusion will impact the path of microstructural evolution.

During the intermediate and final stages of sintering, densification is commonly accompanied by grain growth. Cannon, Yan, and Chowdhry[10] have developed a theory of simultaneous grain growth during densification. The modelling assumes that densification is the result of material transport from the grain boundary to pores via lattice or grain boundary diffusion. Grain growth is assumed to be pore-drag-limited, and therefore the grain growth rate is controlled by the pore mobility. The pore mobility is in turn limited by either vapor transport, lattice diffusion, or surface diffusion. This theoretical framework allows consideration of various combinations of densification and coarsening processes.

Analytical relations have been derived for several limiting cases including: 1) densification controlled by grain boundary diffusion and grain growth limited by either surface diffusion or evaporation and condensation, and 2) densification controlled by lattice diffusion and grain growth controlled by surface diffusion. These relationships provide a means of assessing the effects of changes in the particle size, green density, and the controlling transport mechanism on microstructural evolution via grain size-density plots. Thus, these plots provide a useful tool for identifying controlling sintering mechanisms, and if the sintering mechanism is identified, can suggest changes in the processing conditions that will improve sinterability. In general, the results indicate that benefits that can be derived from increasing the contributions from certain transport processes, and reducing the contribution from others. Several strategies for manipulating the coarsening to densification ratio are discussed in a review by Brook.[13]

With progressive reduction of the particle size, one anticipates that the relative contribution of grain boundary diffusion to densification will increase, and similarly, that the relative contribution of surface diffusion to coarsening will increase. In the final stages of sintering, the limiting case of grain growth controlled by surface diffusion and densification controlled by grain boundary

diffusion will be germane. The analysis by Yan *et al.* shows that the grain size-density trajectory is independent of the initial grain size, but is strongly affected by the ratio of the diffusivities, as expressed in the parameter A, and the initial density. A is defined as

$$A = \frac{176 D_b \gamma_s}{3 \omega D_s \gamma_b} \tag{1}$$

where D_s and D_b are the surface and grain boundary diffusivities, respectively, γ_s and γ_b are the surface and grain boundary energies, respectively, and ω and δ are the effective widths for surface and grain boundary diffusion, respectively. Results indicate that if A is less than unity, substantial grain growth occurs, and theoretical density is approached asymptotically. As a result, high densities may not be reached in practice. If instead A is greater than unity, high densities are reached with very little grain growth. The analysis clearly demonstrates the advantage of increasing the boundary to surface diffusivity ratio.

From an experimental viewpoint, the analytical solutions that have been developed for several limiting cases provide opportunities for interpreting the effects of changes in temperature, sintering atmosphere, particle size, and impurity concentration on the resulting path of microstructural evolution. The results of Berry and Harmer[14] illustrate the application of the principles developed by Yan *et al.* to an assessment of the effect of MgO solute on microstructure development in Al_2O_3.

Microstructural Instabilities

An alternative method of assessing the effects of dopant additions on the competition between densification and coarsening is provided by the work of Shaw and Brook[15] in which the evolution of the pore surface area and grain boundary area in doped and undoped alumina were compared. This work indicated that the interaction between dopants and microstructural heterogeneities played an important role. Coble[16] and Evans[17] considered the effects of inhomogeneities in particle size or of particle packing on sintering. Evans specifically considered stress development due to nonuniform sintering rates, and the potential for defect generation by these stresses. The role of heterogeneities, both microstructural (*e.g.*, packing, particle size, chemical) and inherent (*e.g.*, anisotropic thermodynamic and kinetic characteristics of interfaces) has recently become the focus of greater attention.

Kingery and Francois established the importance of pore coordination number N and dihedral angle ψ on pore stability.[18] The dihedral angle was defined in

terms of the ratio of the surface (γ_s) and grain boundary (γ_b) energies by the relationship

$$\frac{\gamma_b}{\gamma_s} = 2 \cos \frac{\psi}{2} \tag{2}$$

For combinations of ψ and N that satisfy the relationship

$$\psi > (1 - \frac{2}{N})\pi \tag{3}$$

the centers of curvature lie on the vapor or pore side of the solid-vapor interface. Kingery and Francois reasoned that pores satisfying this relationship will shrink. If instead the center of curvature lay outside the pore, the pore would grow.

Cannon reconsidered this problem and reformulated the thermodynamics of pore growth and pore shrinkage.[19] The expressions derived for the chemical potentials which drive pore growth or shrinkage include terms which depend upon the pore curvature, the grain boundary line tension, the applied stress and the pressure within pores. Depending upon the dihedral angle, pore curvature either promoted densification or pore growth. However, the additional grain boundary tension term always favored densification. The analysis predicts that at low dihedral angles ($\psi < 60°$ in two dimensions, $\psi < 70.5°$ in three dimensions), there is no barrier to nucleation of pores and cavities in dense material, and that an equilibrium porosity should develop. At intermediate dihedral angles, pores with low coordination numbers are predicted to shrink and disappear; pores with high coordination numbers are expected to shrink initially, but to reach an equilibrium size at which densification would cease. Cannon argued that grain growth without pore growth would reduce the pore coordination number and promote further densification. A similar conclusion was reached by Lange.[20]

Carter and Glaeser[21] have extended the original analysis of Kingery and Francois, and evaluated the effects of a dihedral angle distribution on pore stability. In a material with a dihedral angle distribution, the dihedral angle will differ among pore-grain boundary intersections. For a pore coordinated by N grains, there are likely to be N unique dihedral angles. The specific dihedral angles sampled will affect the driving force for changes in pore volume (and possibly pore shape). If two N-coordinated pores are compared, the dihedral angles probed will likely differ, and thus, the driving forces for pore shrinkage can differ. To assess the effect of a dihedral angle distribution on the tendency for a pore to shrink or reach a metastable configuration, a condition of pore stability appropriate to a

situation in which the dihedral angles are distributed was derived. The result of the analysis is that pores for which

$$\sum_{i=1}^{N} \psi_i \leq (N - 2)\pi \tag{4}$$

are stable and will resist shrinkage. Several test dihedral angle distributions were assumed, and the dihedral angle sum for N-coordinated pores was assessed. By comparing the dihedral angle sum distribution with the value required for stability, the impact of the selected dihedral angle distribution on the statistical population of stable n-coordinated pores was determined. The effect of changes in the details of the dihedral angle distribution on pore stability was demonstrated by comparing the statistical populations of stable pores for three dihedral angle distributions that either differed in average dihedral angle, or had the same "average" dihedral angle despite having distributions that are highly distinct. The results suggest that the transition from pore shrinkage to pore metastability is not as abrupt as suggested in previous analyses. The differences between the predictions of the isotropic models and one which incorporates dihedral angle distribution effects become more pronounced as the pore coordination number decreases. The results also suggest that changes in processing that reduce surface energy anisotropy can impact sintering beneficially. A similar suggestion has been made by Handwerker and Blendell.[22]

Carter and Cannon have presented a set of exact calculations, pertinent to the sintering of a row of particles with a uniform dihedral angle spanning the range from $\psi = 0°$ to $180°$.[11,12] Equilibrium shapes of segments of a row were calculated for the case where the center-to-center, or interparticle distance, remains fixed. This situation could arise when nondensifying transport modes such as surface diffusion or vapor-phase transport are active, or when the system is constrained. The equilibrium shapes for a fixed dihedral angle differ from those that develop when densification is permitted, that is, when constraint is absent and volume or grain boundary diffusion dominate. The sintering potential Σ, defined as the applied stress required to halt densification, also differs. Local differences in curvature that result from local variations in dihedral angle can provide a driving force for coarsening type processes. The sintering potential Σ was calculated as a function of shrinkage for the case where surface redistribution is sufficiently rapid to produce uniform surface curvatures. Exact expressions for the shrinkage rate for this condition were derived.

The individual processes of coarsening and differential densification, and their interaction in idealized compacts consisting of rows of particles were also considered.[12] For all (fixed) dihedral angles, the curvature of the particle surface always decreases with increasing particle volume, and thus, all systems are prone to a coarsening instability in which sections of the particle chain that have gained an infinitesimal amount of mass continue to gain mass from the adjoining regions of (now) higher curvature. This mass exchange leads to an "undulation" in the cross-section or thickness of the particle chain along its axis. This undulation will then intensify until a particle develops an aspect ratio for which no stable shape exists. This particle then should breakup, producing a discontinuity in the chain.

Differential densification can result when it is energetically favorable to continue densifying one or more grains (at constant volume) at the expense of one (or more) of its neighbors. Carter and Cannon have shown that stability to differential densification requires that the derivative of the sintering potential Σ with respect to length L be positive.[12] Interestingly, for dihedral angles greater than $\approx 120^\circ$, the derivative $\left(\frac{\partial \Sigma}{\partial L}\right)$ is negative for $L \approx L_o$ (where L_o is the initial length). Thus, the system is inherently unstable to differential densification within the grain length range for which the derivative is negative. The sign of the derivative is positive for all dihedral angles near the point at which $\Sigma = 0$; thus, a highly densified system will not be subject to differential densification. A different instability arises if the segment extends to a length sufficiently in excess of L_o.

When both coarsening and densification processes are active, the situation becomes complex. The microstructural instabilities become coupled, and it is possible for one process to either accentuate or mitigate the instabilities arising from the other. Which of these scenarios is valid depends upon the dihedral angle, the geometry, and the constraints imposed on the system. A mapping procedure that identifies regions of accentuating and mitigating interactions in terms of local geometry and dihedral angle parameters has been developed.[12]

2.2 Experimental Opportunities

A theoretical framework for the selection of dopants and sintering atmosphere for sintering control exists.[10] However, in order to use models of the coarsening-densification competition predictively, thermodynamic data, values for materials parameters, and above all, accurate values for the relevant transport coefficients are required. Although the scientific bases for measuring and interpreting lattice diffusivities in most ceramic systems are relatively well established, available grain boundary and surface diffusion data are often contradictory and irreproducible.

The compilation of surface diffusion data in alumina presented by Gupta[23] provides but one example.

The profound disparity in reported surface and grain boundary diffusivities points to a need to develop experiments in which the effects of differences in microstructure, crystallography, chemistry, and other factors on surface and grain boundary transport can be isolated and determined more easily. Lithography provides control over the pore, flaw, or second-phase geometry. The microstructure or chemistry of internal interfaces can be modified or controlled. In some cases, one can alter the relative contributions of coarsening and densification processes. In addition, the same experimental approach provides a means of evaluating dihedral angle distributions as a function of chemistry, and in some cases, the nature of the microstructure. Collectively, these attributes provided the driving force for the development of a series of lithography-based model experiments designed to further our understanding of both the thermodynamics and kinetics of microstructural evolution, and to provide a powerful supplement to more conventional experimental approaches.

These model experiments are based on a modification of lithographic methods used in the semiconductor industry, and subsequent application of the method to ceramics. The majority of the research has focussed on sapphire and alumina, however, the technique can be applied to other crystalline ceramics and to glasses. Figure 1 and the ensuing description summarize the processing steps; a detailed discussion of the experimental method, and its inherent limitations has been published elsewhere.[24,25]

A substrate is coated with a thin layer of photoresist. Controlled geometry structures are computer-generated, and transferred to a chrome oxide mask which is used to selectively expose the photoresist coating. A broad range of feature sizes and shapes can be produced; defect structures can be microdesigned to suit the needs of the particular topic of study. After the exposed pattern has been developed, and the coating has been removed selectively, etching is performed using an argon ion beam in a commercial ion mill. For some materials wet-etching techniques are applicable. Examples of accessible surface structures are illustrated in Figure 2. In addition to producing patterns in which a feature of constant size is repeated (up to 10^6 times), motifs containing pores of varying size (as small as ≈ 0.4 μm equivalent spherical radius) and shape can be created and reproduced.

Controlled surface structures are transferred to an internal interface using hot pressing. Two substrates, one unetched and the other containing the etched-in surface structures, are bonded at elevated temperature. If two single-crystal wafers are bonded, the bicrystal boundary misorientation can be controlled and varied. Single-crystal/polycrystal and polycrystal/polycrystal ensembles can also

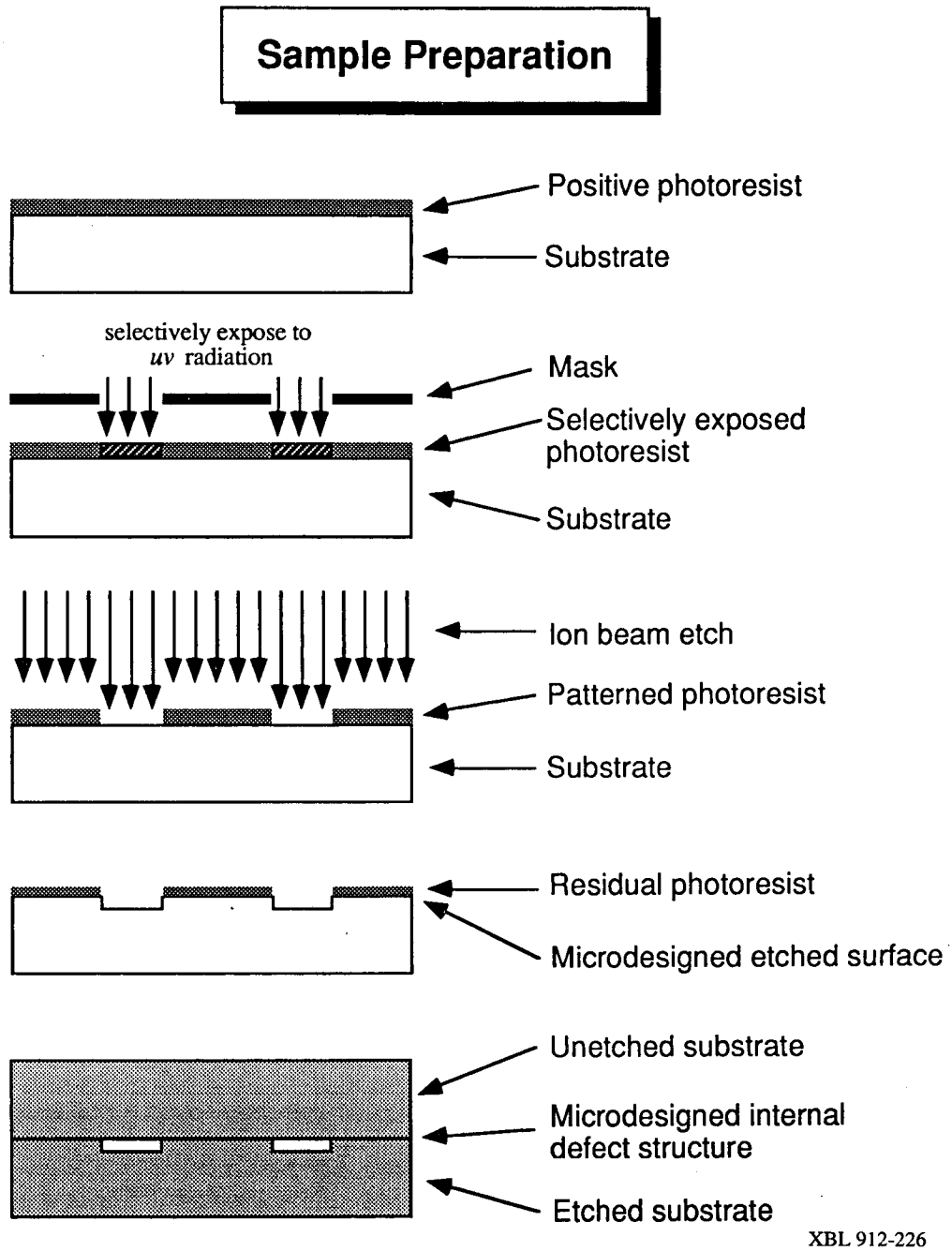

Figure 1 Schematic illustration of processing steps used to prepare microdesigned internal interfacial structures. Top to bottom: photoresist coated substrate; selective exposure of the photoresist; etching of patterned photoresist; microdesigned interface.

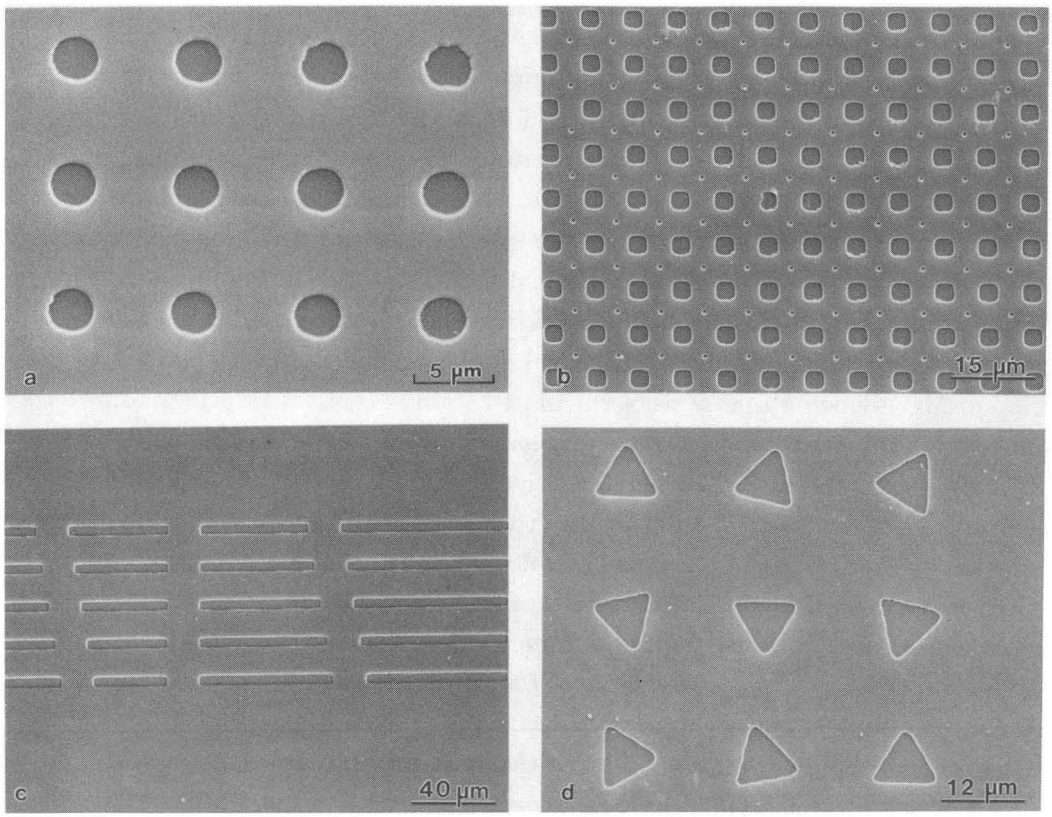

XBB 894-2696

Figure 2 Examples of lithographically introduced surface defects prior to transfer to an internal interface by hot pressing: a) monosized pore arrays, b) bimodal pore arrays, c) pore channels used for Rayleigh instability studies, and d) rotated triangle for sampling differing flaw edge crystallographies.

be produced. The former provides a means of studying abnormal grain growth and pore-boundary interactions; the latter most closely allows simulation of defects in polycrystalline materials. Conditions promoting good bonding have been identified, leading to the fabrication of continuously bonded ensembles, with interfacial structures reflecting etched surface structures.

Dihedral Angle Measurements

The dihedral angle formed at the junction between a grain boundary and free surfaces plays an important role during essentially the entire sintering process. It affects the geometry of interparticle necks and the equilibrium shapes (curvature) of particles; the dihedral angle and its distribution will impact the susceptibility of a material to coarsening and differential densification. In the final stage of sintering, the dihedral angle together with the pore coordination number dictates the geometry of intergranular pores, and thus, plays a key role in defining the

driving force for densification and pore closure. In the final stage of sintering (as discussed in a later section), the dihedral angle impacts the peak pore velocity,[26] and thereby, pore-boundary separation conditions. As a result, there is considerable utility in measuring dihedral angle distributions in ceramics.

Recently, Handwerker *et al.* have reported a new high resolution technique utilizing lithographically introduced metal reference lines (MRL) for measuring the dihedral angle formed at surface thermal grooves.[27] As the resolution of the technique increases, one expects the measured dihedral angle to decrease and approach the true dihedral angle. Dihedral angles on the same thermally grooved surface of MgO-doped alumina were calculated from: 1) optical interferometry data obtained from the groove root, 2) measurements of the groove width by applying models of surface diffusion dominated thermal grooving, and 3) SEM measurements of MRLs that conformed to the shape of the groove. A comparison of the results showed the expected trend in values; the use of the MRL technique resulted in a dihedral angle distribution that was shifted to lower values in comparison to those obtained using the other two methods.

In a companion paper,[28] Handwerker *et al.* report the application of the method to measurements of dihedral angles in Al_2O_3, MgO-doped Al_2O_3, and MgO. The results indicate that MgO-doping reduced the spread in the dihedral angle distribution in alumina. This would be expected to lead to a more uniform driving force for densification, a more uniform transition from the intermediate to the final stage of sintering, and a more uniform peak pore velocity. There are other benefits to MgO-doping, and additional benefits are continuing to be found, however, the aforementioned set of benefits can be anticipated from a change in the width of the dihedral angle distribution.

The technique for measuring dihedral angles developed by Handwerker *et al.* utilizes lithographic methods to introduce the metal reference lines at external surfaces. Lithographic processing can also be used to generate controlled arrays of internal pore channels, and these channels may also be useful in measuring dihedral angles. Specifically, long pore channels can be introduced into a polycrystal surface. This etched polycrystal can be bonded to a second polished polycrystal. Depending upon the pore channel width/diameter (which can be controlled) and the local grain size, the pore channels will lie at the intersection of two or more grains and will adjust their shape accordingly. Following high temperature anneals, sections orthogonal to the pore channel axes can be prepared and studied using scanning electron microscopy. The groove angle can be measured, and in addition, by thermally etching the specimen and correlating the microstructure with the appropriate pore channel, it should be possible to assess whether groove asymmetry is due to torque terms or the inclination of the grain

boundary to the pore. The application of this method to alumina is currently being pursued.[29]

Pore Coarsening and Pore Elimation Studies

By utilizing lithography, arrays of micron and submicron equivalent spherical diameter pores can be introduced at an internal interface. Both monomodal and bimodal arrays can be produced. Figure 3 illustrates controlled-geometry bimodal pore arrays; Figure 4 shows corresponding optical micrographs of bonded specimens. By isolating arrays of specific pore size and spacing with pore-free regions several hundred microns in width, pore shrinkage during bonding/hot pressing can be reduced significantly. If this pore-free border is retained, coarsening will occur during subsequent annealing. If instead the pore-free region is removed following bonding, studies of pore shrinkage during sintering or hot pressing are possible.

During final stage sintering, vacancies are redistributed from pores to either larger pores or to the grain boundary. The dominant vacancy sink determines whether coarsening (pore sink) or densification (grain boundary sink) results. However, diffusion through the lattice and along the grain boundary occurs in both cases. Thus, when diffusion is rate controlling, measurements of the coarsening or densification rates can be used to deduce the diffusivities for lattice and grain boundary transport, D_l and D_b, respectively. Measurements performed on zero-misorientation bicrystals can be used to assess the lattice diffusion contribution to coarsening or densification. Since the grain boundary misorientation can be controlled in a bicrystal, the grain boundary diffusivity for a grain boundary of specific misorientation can be measured. If polycrystalline samples are used, a statistically averaged grain boundary diffusivity can be determined. Alternatively, interfacial reactions involving the annihilation of vacancies at grain boundaries,[30-32] or the annihilation or creation of vacancies at pore surfaces[33] may be rate controlling.

Several specific applications of the method have been suggested.[34] The ability to control the volume fraction, size, size distribution and spatial distribution of interfacial pores, and to vary each of these parameters systematically over wide ranges allows essentially complete control over the topological characteristics that can affect coarsening and densification rates. As a result, the effects of changes in the topological characteristics on sintering can be studied. If comparisons of coarsening or densification rates in zero and finite misorientation bicrystals indicate a substantial contribution from grain boundary diffusion, it may be possible to extract absolute values for the grain boundary diffusivity. One advantage of a diffusivity determined from measurements of this type is that the

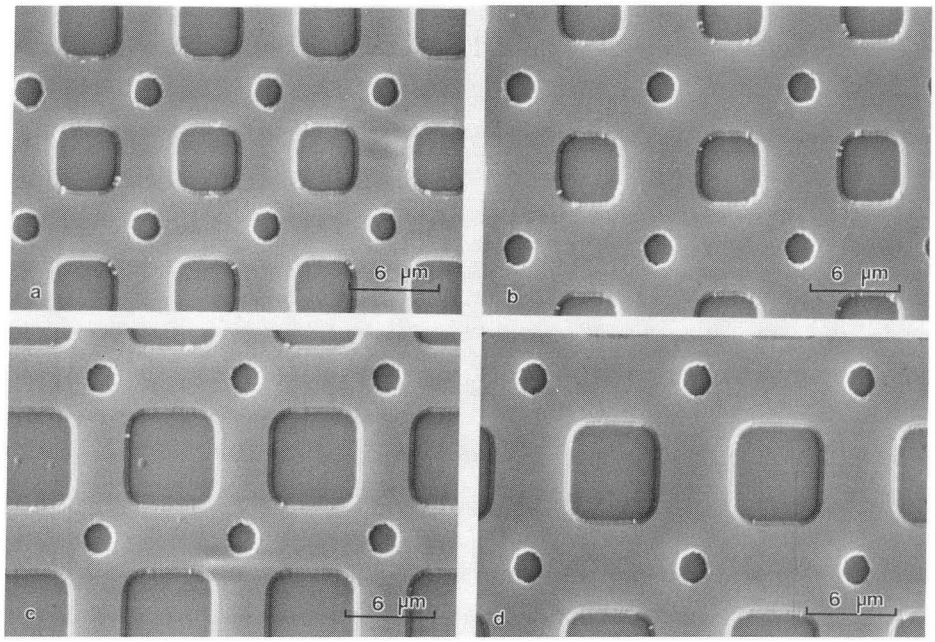

XBB 878-6527A

Figure 3 SEM micrographs of bimodal pore arrays prior to bonding. Large pores have widths of (a,b) 4 μm and (c,d) 6 μm; width of the small pores is 2 μm in all figures. The center-to-center pore spacings (large-small pore pairs) are a) 6 μm, b,c) 8.5 μm, and d) 10 μm.

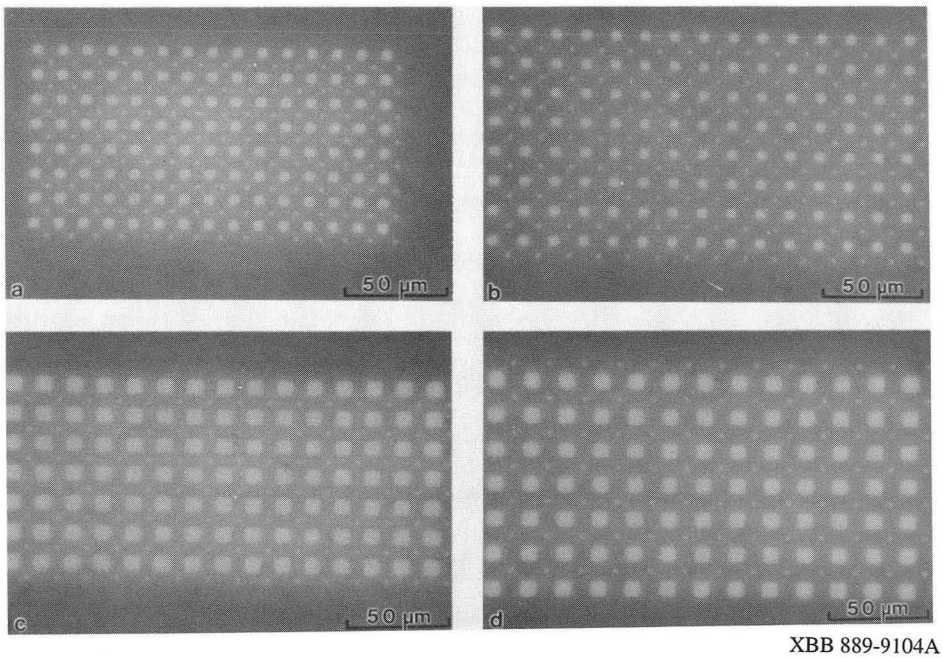

XBB 889-9104A

Figure 4 Optical micrographs of bimodal pore arrays in Figure 3 after bonding.

values are deduced from kinetic measurements of the process of specific interest. Since the boundary misorientation and pore pattern can be reproduced and introduced into undoped and doped crystals, a clear assessment of the effects of dopants on grain boundary transport should be possible. Experiments can be tailored to maximize the possibility of interfacial reaction control. The effect of hydrostatic stress on vacancy annihilation at grain boundaries can also be determined. Changes in the stress dependence of the pore elimination rate can serve as an indicator of a transition from interfacial reaction rate control to diffusion control. In summary, lithography provides a powerful new tool for studying the role of interfaces during densification and coarsening.

Pore and Defect Morphology Evolution

Studies of pore and defect morphology evolution can be used to provide kinetic information, thermodynamic information, or both. Lithographically introduced defects are well suited to addressing a wide range of problems including: determination of equilibrium and metastable pore morphologies, the morphological instability of pore channels and pore networks, high-temperature crack healing, and the evolution of defects at ceramic-ceramic and ceramic-metal interfaces during diffusion bonding.

Lithography provides a convenient way of introducing large number of pores at an internal interface of controlled misorientation. Measurements of the pore shapes that evolve as a result of extended high-temperature annealing provide information on the form of the surface energy γ_s versus surface orientation plot.[35,36] Both intragranular and intergranular pore structures can be produced.[37]

Studies of pore channel morphology evolution provide insights on the effect of surface energy anisotropy on microstructural evolution, and in some materials may be useful for measuring the surface diffusion coefficient. Pore channels of varying aspect ratio have been introduced at grain boundaries in low misorientation angle sapphire bicrystals. By interspersing anneals and characterization using optical microscopy, the evolution of the pore channels was studied.[38] The breakdown characteristics, *i.e.*, the perturbation wavelengths and ultimate pore-pore spacings, suggest strong effects of surface energy anisotropy even at 1800°C. Previous experimental approaches have offered limited control over crack face and crack edge crystallography and grain boundary misorientation. Variations in these parameters may contribute significantly to the wide disparity in the surface diffusivities inferred from rates of pore channel breakup.

Studies of high-temperature crack healing in sapphire also indicate that crack face crystallography and crack edge orientation have a major impact on the healing process. Cracks oriented parallel to the basal, prismatic, and rhombohedral planes exhibit distinct healing patterns.[39,40] Recent results by Baik and co-workers

indicate that segregation of calcium to surfaces and grain boundaries in alumina is anisotropic.[41,42] High temperature crack healing experiments may provide a convenient means of determining how this impacts the transport properties.

3. GRAIN BOUNDARY MIGRATION AND PORE-BOUNDARY INTERACTIONS

Microstructural characteristics often reflect grain boundary migration during processing and high-temperature service. Thus, property optimization through control of microstructural evolution requires that the driving force, temperature, and composition dependencies of grain boundary migration rates be known. Ceramics invariably have dissolved impurities, and may also contain pores, second phase particles, and liquid phases. Each can affect boundary migration rates, and under certain conditions, may control migration behavior.

During the final stage of sintering, the interaction between pores and grain boundaries is particularly important. Whether pores and boundaries remain attached or separate often determines whether complete densification is possible. Pore attachment requires that the velocity of the pore-laden not exceed the so-called "peak pore velocity."[26] In principle, one method of promoting attachment is to introduce dopants that segregate to and reduce the grain boundary mobility. A comparison between grain boundary migration rates in doped and undoped dense material should provide a simple means of assessing the effect of the dopant on the grain boundary mobility, the velocity per unit driving force.

Prior to 1975, there were few studies using ceramics in which pore-boundary, precipitate-boundary, or solute-boundary interactions had been *isolated* and systematically investigated.[43] During the last fifteen years, this deficiency has been addressed by many careful studies. Modelling of pore-boundary interactions has also advanced, and until very recently, the models were more refined than the experimental methods available to test them. The objective of this section is thus to summarize some of the modelling and modelling advances, to identify some of the key experimental observations, and also to indicate areas where further work is needed.

3.1 MODELLING

The Grain Boundary Mobility

Two extremes of migration behavior are possible as a result of solute-grain boundary interactions in a single-phase material. Weak solute-boundary interactions have a minimal effect. A migration rate like that in an ideally pure material having the same driving force for migration F_b is expected. This extreme defines the maximum migration rate, the intrinsic rate. In contrast, a reduced migration rate is expected when the solute-boundary interaction is strong. The

associated steady-state behavior, referred to as stable solute drag limited (SDL) migration, defines a minimum migration rate (in a single-phase material). If transitions between these behavioral extremes can occur, intermediate (time-averaged) boundary velocities can be observed.

Since both the intrinsic and SDL boundary velocities depend on F_b, and may vary widely, it is convenient to normalize the boundary velocity V_b, and compare the boundary mobility M_b, defined as

$$M_b = \frac{V_b}{F_b} \tag{5}$$

This simplifies distinguishing between cases in which a difference in F_b has produced only a velocity difference, and those in which the mechanism has also changed. A driving force induced change in migration mechanism changes both the magnitude and temperature dependence of M_b; when V_b alone is changed, M_b may remain constant at fixed temperature.

Intrinsic Migration

An upper limit for the intrinsic mobility may be obtained by assuming that V_b is limited only by the rate of ion transfer across the boundary by diffusional jumps. The intrinsic mobility M_o, can be approximated by a modified version of the relationship derived by Turnbull,[44]

$$M_o = \frac{V_b}{F_b} = \frac{f D_b \Omega}{lkT} \tag{6}$$

where D_b is the boundary self-diffusion coefficient for the slower ion for transport normal to the boundary plane; Ω, the total volume divided by the number of slow diffusing ions; l, the boundary core width, and kT has its usual meaning. The site factor f, reflects the density of boundary core sites associated with high jump probabilities. For random high angle boundaries with poorly ordered core structures, values of $f \approx 1$ are assumed appropriate. Boundaries having ordered core structures due to a special misorientation relationship are expected to have lower intrinsic mobilities. Low angle boundaries are expected to have much lower mobilities. Measurements of intrinsic grain boundary mobilities in ceramics are, at best, rare. For a boundary of fixed structure, M_o must be driving force independent.

Solute Drag Limited Migration

The solute drag force F_s from a segregated solute cloud depends on the solute distribution and its motion relative to the boundary. This problem has been treated

by Cahn[45] as well as Lücke and Stüwe,[46] and extended to ionic materials by Yan.[47] An approximate solution for steady-state migration given by Cahn[45] is

$$F_s = \frac{\alpha C_\infty V_b}{(1 + (\beta V)^2)} \tag{7}$$

where α is the solute drag force per unit velocity and per unit solute concentration in the low-velocity limit, C_∞ the bulk solute concentration, and β^{-1} is approximately the velocity with which a solute diffuses across the near grain boundary region. The drag coefficient α depends on temperature, the solute diffusivity in the near grain boundary region, and the absolute magnitude of the solute-boundary interaction energy.

During steady-state migration, the total drag force F_t acting on a boundary is equal to the imposed driving force F_b, and is assumed to be the sum of F_s and F_o, the intrinsic drag force. Thus,

$$F_t = \frac{V_b}{M_o} + \frac{\alpha C_\infty V_b}{1 + (\beta V_b)^2} \tag{8}$$

At sufficiently low F_b, $(\beta V_b) \ll 1$. If in addition $F_s \gg F_o$,

$$F_t \approx \alpha C_\infty V_b \tag{9}$$

Thus, in the high drag, low velocity limit, M_b should be proportional to $1/C_\infty$, independent of F_b, and have an activation energy nearer that for bulk diffusion than for boundary diffusion.

The Pore Mobility

Like grain boundaries, pores and particles can also migrate under an imposed driving force. Shewmon addressed the problem of inclusion movement in response to temperature gradients.[48] Nichols extended the model to consider the migration of pores with grain boundaries during grain growth in porous compacts.[49] The interactions between pores and migrating boundaries differ in two important respects from those characterizing solute-boundary interactions:[43] 1) the drag force due to pores is spatially nonuniform whereas that from a (uniformly distributed) solute should be more nearly uniform, and 2) the pore mobility is frequently much slower than the impurity diffusion.

A pore "attached" to a grain boundary, and thus "dragged" by the moving boundary, migrates at a velocity that depends upon the transport path of atoms through or around the pore. The expressions for the pore mobility have the form

$$M_p = A\frac{\exp(-\Delta G_i / kT)}{r^n} \tag{10}$$

The exponent n of the pore radius r depends upon the transport process and assumes a value of 3 for lattice diffusion, 4 for surface diffusion, and a value of either 2 or 3 for vapor transport. The activation energy ΔG_i will reflect the particular transport process. For the specific case of surface diffusion controlled pore migration, the approximate pore mobility obtained in this way is given by

$$M_p = \frac{D_s \delta_s \Omega}{kT\pi r^4} \tag{11}$$

where $D_s\delta_s$ is the product of the surface diffusivity and the surface thickness and Ω is the atomic volume.[48]

The drag force exerted by the grain boundary on the pore was also estimated by considering the pore to remain spherical during motion. By allowing the contact line between the pore and the grain boundary to move freely over the pore surface, a maximum driving force for pore migration emerges.

$$F_p = \pi r \gamma_b \tag{12}$$

where γ_b is the grain boundary energy. The product of the pore mobility and the maximum driving force for pore migration defines the peak pore velocity.

Hsueh *et al.* addressed the shape changes that were necessary to maintain an atomic flux over the pore surface during pore migration via surface diffusion.[26] The results indicate that the dihedral angle plays an important role in modifying the peak pore velocity. The predicted steady-state peak pore velocity was approximated as

$$v_p \approx \frac{\Omega D_s \delta_s \gamma_s}{kTr^3}(17.9 - 6.2\psi) \tag{13}$$

where ψ is the dihedral angle. The analysis indicates that for all reasonable dihedral angles the steady-state velocity exceeds the peak pore velocity estimated for a spherical pore. It is noteworthy that the equation also provides a means of determining a surface diffusion coefficient relevant to microstructural changes during sintering if the peak velocity of a pore of known size can be measured.

Pore-Boundary Interactions

Brook was the first to analyze pore-boundary interactions, and to develop a mapping procedure identifying conditions of pore attachment and pore separation. The treatment of pore-boundary attachment and separation focuses on a comparison of the relative values of the *peak* pore velocity v_p and the velocity of the pore-laden grain boundary $v_{b(p)}$.[50,51] Attachment requires that

$$v_p = v_{b(p)} \tag{14}$$

The velocity of the pore-laden grain boundary is the product of the boundary mobility M_b and the driving force on the boundary F_b diminished by the drag force exerted by the pore array NF_p

$$v_{b(p)} = M_b(F_b - NF_p) \tag{15}$$

where N is the pore density, and F_p is the drag force exerted per pore. (F_p is also the driving force for pore migration.) This result can be rearranged to yield

$$v_{b(p)} = F_b \frac{M_b M_p}{NM_b + M_p} \tag{16}$$

Two limiting cases emerge from this analysis. In the first, $NM_b \gg M_p$, which yields

$$v_p = v_{b(p)} = \frac{F_b M_p}{N} \tag{17}$$

Since the boundary velocity can also be expressed as $(F_b\text{-}NF_p)M_b$, it follows that in this case the net driving force acting on the boundary is small, *i.e.*, the driving force on the boundary is nearly balanced by the drag forces from the pores. In this situation, the boundary motion is limited by the pore mobility.

The second limiting case of interest occurs when $NM_b \ll M_p$. This yields

$$v_p = v_{b(p)} = F_b M_b \tag{18}$$

This result, in conjunction with the basic equation describing attachment, Eq. 14, indicates that for this situation

$$NF_p \approx \frac{NM_b}{M_p} F_b \ll F_b \tag{19}$$

Thus, the driving force for grain boundary migration exceeds the total drag force exerted by all pores, and the grain boundary velocity is dictated by the boundary mobility.

Separation occurs when the grain boundary velocity exceeds the peak pore velocity. The peak pore velocity in turn is the pore velocity under the maximum applied driving force, $\approx \pi r \gamma_b$. In the context of Eq. 15, a critical driving force for pore-boundary separation can be defined. Separation is predicted when

$$F_b > (F_p)_{\max}\left(N + \frac{M_p}{M_b}\right) = \pi r \gamma_b \left(N + \frac{M_p}{M_b}\right) \tag{20}$$

The driving force F_b is due to grain boundary curvature, and is usually assumed to scale inversely with the average grain size. High pore densities, and a high pore mobility to boundary mobility ratio increase the driving force range within which pores remain attached to boundaries. Understanding the role of additives on pore boundary separation is complicated because solute additions can affect the pore mobility (*e.g.*, the solute may increase or decrease the surface diffusion coefficient), and at the same time, can affect the grain boundary mobility via solute-boundary interactions.

3.2 Experimental Progress and New Opportunities

There have been numerous measurements of grain growth rates in a wide range of ceramic systems. In many cases, the measured grain growth rates were affected by second phases, *e.g.*, pores, precipitates, intergranular liquids. An exhaustive review of the grain growth literature through approximately 1975 was presented in a review paper by Yan *et al.*[43] This review remains perhaps the most comprehensive source of grain growth data for ceramic systems. The objective of the ensuing section is to discuss selected recent work addressing grain growth in ceramic systems. One topic of interest and importance is the effect of solutes on

grain boundary migration. It follows from the modelling developed by Brook, that dopants that reduce the grain boundary mobility can extend the range of pore-boundary attachment, and thereby, increase the likelihood of achieving high density. The specific consideration of pore-boundary interactions is also of interest. Recent work addressing this problem will also be reviewed.

Solute Drag

To isolate the effects of solute additions on grain boundary migration rates, it is desirable to perform experiments on materials containing no second phases. One method of achieving this is to perform recrystallization experiments on deformed single crystals. This approach was pioneered by Müller[52] (in the 1930's!) and was used to characterize grain boundary migration rates in NaCl. This method was adopted by Yan,[53] and subsequently by Glaeser *et al.*,[54] to investigate the effects of isovalent and aliovalent dopants on grain boundary migration rates in alkali halides. The Sun and Bauer method,[55] which relies on the growth of controlled misorientation bicrystals from the melt, provides an alternative approach to isolating solute-boundary interactions, and can be used to identify effects of grain boundary misorientation on grain boundary mobility. To the author's knowledge, this method has been applied to a number of metallic systems*e.g.*,[56,57], but application to ceramics is limited to NaCl[58] and KCl.[59]

The results obtained from grain boundary migration studies in undoped alkali halides suggested that intrinsic grain boundary migration rates were rarely if ever achieved even in these highly pure systems. At temperatures approaching the melting point, mobilities expected for intrinsic migration were *approached*. At lower temperatures, observations of sustained migration at intrinsic rates were isolated and generally not reproducible. Dopant additions reduced the grain boundary mobility. The extent of mobility reduction was dependent upon two factors: 1) size misfit, and 2) charge misfit .[53,54,59] Specifically, for isovalent dopants, those with a larger size mismatch appeared to produce a more significant reduction in the mobility.[53,59] However, the results generally suggest that aliovalent impurities have a much more significant impact on the mobility than isovalent impurities.[53,54,59] For additions of Na, Mg, and Al to LiF,[54] the solute drag coefficients (Eq. 9) differed greatly with $\alpha_{Al}/(7 \times 10^4) \geq \alpha_{Mg} \geq 5\alpha_{Na}$. If the results obtained in LiF can be considered characteristic of highly ionic, stoichiometric compounds, the results suggest that aliovalent impurities at the ppm level can dominate grain boundary migration characteristics. This is not inconsistent with the observation that most observed grain boundary mobilities for oxides fall well below the calculated intrinsic values.[43]

The experimental approaches used to measure grain boundary mobilities in alkali halides do not lend themselves to measurements of grain boundary mobility

in more refractory and less plastic oxide materials. Either the temperatures needed to activate a sufficient number of slip systems to permit flow without failure are very high, or thermal expansion anisotropy complicates the growth of bicrystals. In general, two experimental approaches have been used to study grain boundary migration in oxides. In the first, large seed crystals have been introduced into a powder compact[*e.g.*,60,61], or bonded to an already densified compact. [*e.g.*,62] The cited work focussed on identifying the effect of MgO on grain growth rates in alumina. This approach can also be utilized to study the effects of an intentionally incorporated liquid phase on the growth rate and morphology of the seed crystal.[*e.g.*,63,64]. The second approach has focussed on measuring the growth characteristics of the average grain in a polycrystalline matrix. Such experiments do not provide information on grain boundary mobility variations for boundaries of fixed misorientation (*e.g.*, transitions between higher and lower mobilities in response to driving force variations) or boundary-to-boundary mobility differences linked to misorientation differences. However, the experiments can provide valuable information on trends in an average mobility. As an example, recent work by Bennison and Harmer[65,66] has helped to clarify the influence of, and interaction between, a glassy phase and MgO-dopant on grain growth in alumina.

Grain growth continues to be a topic of interest within the field, and there have been numerous excellent papers published on the subject subsequent to the review presented by Yan *et al.*[43] The objective here is to focus on papers that have brought to light some important new aspect to the problem of understanding and characterizing solute-boundary interactions, and identifying some of the underlying factors that have in some systems contributed to significant disparities in the measured grain growth rates. Four contributions will be afforded special consideration.

Bennison and Harmer[65,66] conducted very careful measurements of grain growth rates in dense, doped and MgO-doped alumina, in an effort to identify the role of MgO on grain boundary migration rates. In their initial work, MgO additions (200 ppm) reduced the grain boundary migration rate of the "average" boundary by a factor of approximately five at 1600°C. Subsequently, concerns emerged that the alumina used actually contained a liquid phase. This prompted a re-examination of grain growth in undoped and MgO-doped alumina. When a higher-purity alumina powder was used, the same addition of MgO resulted in a factor fifty reduction in the grain boundary mobility. The results suggest that some of the inconsistencies regarding the effects of specific dopants on grain boundary migration (or other aspects of microstructural evolution) may be the result of the presence or absence of grain boundary phases. Glassy phases of differing composition will have different transport characteristics, and both the transport

and wetting characteristics of the glasses may differ in their response to temperature and dopant additions.

Although grain boundary migration characteristics of highly stoichiometric alkali halides and oxides can be extremely sensitive to background impurities and intentional additives, there is at least system in which the migration characteristics appear to be remarkably impurity tolerant.[67] Magnesium aluminate spinel is a model ternary oxide in which large native defect populations can be achieved by adjusting the stoichiometry. For nearly stoichiometric spinel ($MgO{\cdot}nAl_2O_3$ with $1 < n < 1.07$) materials from a variety of sources and prepared from different starting materials have grain boundary mobilities that agree to within a factor of five at constant temperature. A change in boundary mobility with change in cation stoichiometry is found. It is suggested that unlike the behavior observed in highly stoichiometric ionic systems, the rate limiting species are intrinsic lattice defects that accommodate lattice nonstoichiometry, rather than background impurities or added solutes.[67]

Hwang and Chen have recently investigated the effects of divalent to pentavalent cation dopants on grain growth kinetics and grain-boundary segregation in tetragonal zirconia polycrystals (TZP) with either 12 mol% CeO_2 (12Ce-TZP) or 2 mol% Y_2O_3 (2Y-TZP).[68] The dopants studied included Ca, Mg, Y, Yb, In, Sc, Ce, Ti, Ta, and Nb. Additive levels in the 12Ce-TZP were fixed at 1% substitution of the cation sites, and at 0.6% in the 2Y-TZP. These levels are significantly higher than those used in studies of aliovalent impurity additions in alkali halides, and in studies examining the effects of MgO additions on grain boundary migration in alumina. Moreover, the levels are sufficiently high that extrinsic defects dominate. For the dopants in 12Ce-TZP, the final grain sizes increased with dopant as follows:

$$Ca^{2+} < Mg^{2+} < Y^{3+} < Yb^{3+} < In^{3+} < Sc^{3+} < Ce^{4+} \text{ (base composition)}$$
$$\leq Ti^{4+} < Ta^{5+} \leq Nb^{5+}$$

For the divalent through isovalent dopants, the computed grain boundary mobilities span more than three orders of magnitude. The results of this work indicate that charge mismatch was the dominant factor affecting mobility, and that for dopants of identical charge, larger cations had a more important effect. These results parallel the findings of Yan,[53] Kitazawa *et al.*,[59] and Glaeser *et al.*[54] on alkali halides, and indicate that modelling work of Yan *et al.*[47] which applies the space charge concept to grain boundary migration and solute drag may provide a useful framework for understanding and predicting the relative effectiveness of dopants in some systems.

Normal grain growth measurements inevitably involve averaging. There are situations in which knowledge of only the average behavior is inadequate, and the factors that affect the anisotropy of grain growth, and control not only the size and

size distribution, but also the evolution of the grain shape and grain shape distribution are of interest. Microstructures comprised of columnar or platelike grains may have advantageous mechanical properties, and thus, it is desirable to develop an understanding of the factors that promote anisotropic grain growth. In parallel, effects of grain boundary structure on solute-boundary interactions have been cited in the metals literature;[e.g.,69] orders of magnitude differences in grain boundary mobilities are indicated in some matrix-solute systems. Boundaries having "special" misorientation are "impurity tolerant" in the sense that their mobilities are not as strongly affected by solute additions as more "general" boundaries are. Comparable data for ceramic systems is lacking. More generally, data addressing the width of the grain boundary mobility distribution and the effects of dopants on the distribution of mobility is lacking.

Recently, Rödel and Glaeser studied the migration of single crystal sapphire seeds of controlled orientation into both MgO-doped and undoped polycrystalline aluminas.[70] Large lithographically introduced markers defined the initial position of the sapphire/alumina interface. These reference markers facilitated accurate measurements ($\approx\pm 0.5$ μm) of the seed displacement . Both the migration rate of the sapphire/alumina interface *and* the growth characteristics of the alumina matrix were determined.

Several results are noteworthy. The uniformity and rates of seed migration rates for prismatic plane and basal plane seeds into undoped alumina differed significantly. Growth of the prismatic plane seed was highly nonuniform. Since the nonuniformity exceeded that which would be attributable to local driving force variations along the growth front (and was significantly higher than than that for a basal plane seed growing into a microstructurally similar polycrystal), the results may indicate the effects of local grain boundary orientation on migration characteristics. In a compact, such nonuniformities could promote either abnormal grain growth, pore-boundary separation, or both. The effect of the dopant addition on the migration characteristics also depended upon the seed orientation. MgO additions had little if any discernable effect on the mobility of the basal plane seed. In contrast, MgO additions had a strong homogenizing effect on the mobility of the prismatic-plane seed. Experimental work extending this method to other systems or other dopants, or both, could begin to provide some useful information on grain boundary misorientation specific solute-boundary interactions. Such studies would have particular value if coupled with analysis of interfacial chemistry.

The growth characteristics of the matrix grains was determined to allow a proper accounting of the time dependence of the driving force for seed migration when calculating the seed mobility. Interestingly, the grain boundary mobilities of

the seed crystal and the matrix grains differed, and their ratio was time dependent. Monahan and Halloran[61] and Kinoshita[62] had also studied growth of single crystal seeds into a polycrystalline alumina matrix. Their results also indicate differing grain size and time dependencies for the mobilities of the undoped matrix grains and seeds growing into undoped material; however, they differ in from the results obtained by Rödel and Glaeser. In Kinoshita's work, grain growth in the undoped matrix was described by an approximately cubic growth law, while the rate of seed growth into undoped alumina appeared to be independent of time, and therefore independent of driving force.[62] Monahan and Halloran observed a similar time-independent growth rate of the seed into undoped alumina.[61] In both cases, introduction of MgO led to a reduced rate of matrix grain growth and a decaying (driving force dependent) rate of seed growth. The origin of such differences in behavior is uncertain, however, time (driving force) dependent mobility ratios for abnormal and matrix grains may be more widespread, and may be an additional factor contributing to the *onset* of abnormal grain growth. Further exploration of normal and abnormal grain growth may provide an improved understanding of the driving force dependence of the grain boundary mobility.

Pore-Boundary Interactions

As discussed previously, the essential parameters in models of pore-boundary interactions include the grain boundary mobility, M_b, the pore mobility, M_p, and the areal density of pores. The mobilities can in principle be assessed by measuring grain boundary and pore velocities under known driving forces. The latter is the more difficult to achieve. In addition, the size and areal density of pores is nonuniform in a typical powder compact, and can be difficult to assess in a conventional two-dimensional section.

As a result of these experimental difficulties, there have been relatively few studies of pore-boundary interactions; until recently, pore-boundary separation maps had been obtained only for MgO. Handwerker *et al.* measured the sizes of grains and of attached and separated pores on polished surfaces and found good correlation between predicted and observed behavior.[71] This method is straightforward, however, great care must be taken in obtaining three-dimensional pore and grain sizes from two-dimensional micrographs. In addition, one is limited to investigating pore and grain size regimes that arise naturally during the course of sintering. A similar study by Sakarcan *et al.*[72] utilized measurements of the shapes of distorted pores attached to migrating grain boundaries to examine pore-boundary interactions and predict the critical pore size for separation. This experimental approach also requires great care in sectioning and data interpretation. These experimental uncertainties, coupled with numerous

simplifying assumptions inherent to the analysis, limited the precision with which the critical pore size could be defined.

A model experiment that facilitates the study and characterization of pore drag and pore-boundary was needed. Ideally, such an experiment should have the ability to suppress completely interference from densification, and should allow complete and precise control over the critical geometric parameters that affect pore-boundary interactions, such as pore size, pore spacing, and grain size. Recently, a method satisfying these requirements was developed,[73,74] and has permitted what are termed controlled pore drag experiments. The method has been applied to a study of pore drag and pore-boundary separation in both undoped and 250 ppm MgO-doped alumina.[74]

Controlled pore drag studies utilize photolithographically-introduced controlled-geometry interfacial pore structures.[24] Arrays of monosized (width = 3 μm, depth = 0.24 μm) cavities were formed on the surfaces of either basal-plane or prismatic-plane orientation sapphire. The center-to-center spacing was varied (4, 6, 8, and 10 μm) to modify the drag force exerted on the boundary. Pore arrays 20 pores wide and 1800 to 4000 pores long, with interarray spacings of 200 μm were produced.

To study pore-boundary interactions in alumina, these pore structures were transferred to the interface between single-crystal sapphire and dense polycrystalline alumina by hot-pressing the etched sapphire wafers against dense highly polished dense MgO-doped or undoped alumina polycrystals. The polycrystals were fabricated by a two-stage hot-pressing hot-isostatic-pressing process designed to achieve theoretically dense, fine grain size alumina. Wide pore-free ligaments surrounding pore arrays were used to essentially eliminate densification during hot pressing and annealing. An example of a controlled-geometry interfacial pore structure after bonding, but prior to any high-temperature annealing is provided in Figure 5.

During subsequent heat treatment of the bonded ensemble, the single-crystal seed will grow into and consume the polycrystalline alumina. Experiments in which the growth of unetched (pore-free) sapphire wafers into both undoped and MgO-doped alumina polycrystals was monitored provide information on the migration characteristics in the absence of pore-boundary interactions. Combined with measurements of the grain growth kinetics, the velocity-driving force relationship for the interface can be determined. The conditions under which pores remain attached to a migrating interface, as well as the critical condition for pore-boundary separation can be determined by monitoring the growth of an etched sapphire wafer (containing controlled-geometry pore arrays) into the same undoped and MgO-doped alumina polycrystals.

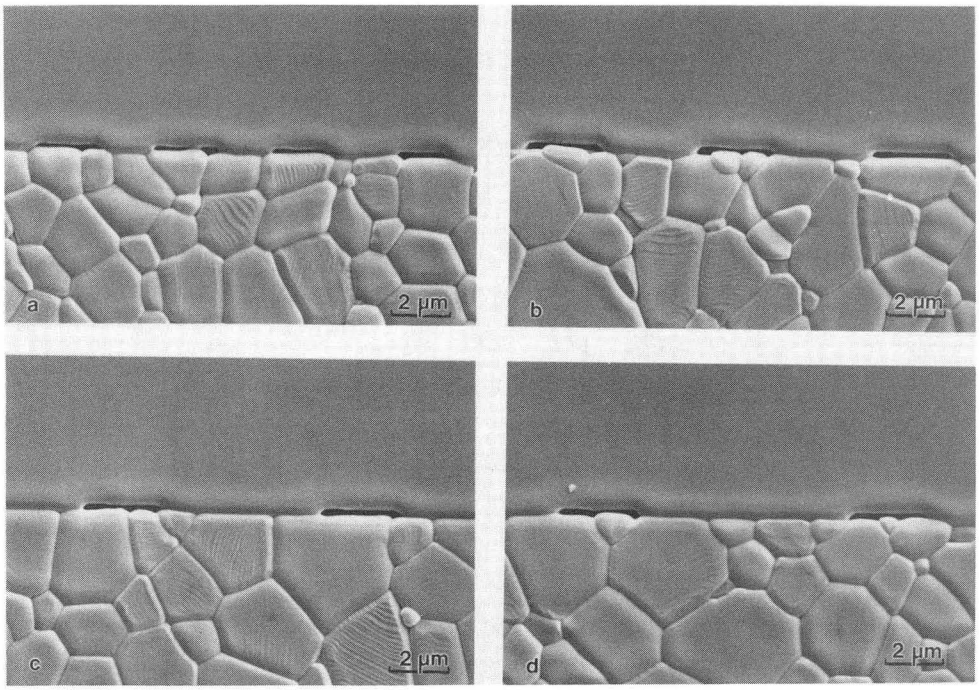

XBB 882-742

Figure 5 SEM micrographs of microdesigned interface containing monosized pores of varying center-to-center spacing: a) 4 μm, b) 6 μm, c) 8 μm and d) 10μm.

Following an initial period in which the shape of the interfacial porosity adjusts from being like that of a crack to that of a more equiaxed intergranular pore, migration of the pore-laden interface initiates. During this subsequent migration, pore either remain attached to the migrating interface and $V_b=V_p$, or under some conditions, the boundary velocity exceeds the peak pore velocity, results in pore-boundary separation, and isolation of the pore arrays within the growing single-crystal sapphire seed. The migration kinetics of the single-crystal/polycrystal interface reflect the size and spacing of the pores comprising the interfacial pore arrays. Figure 6 illustrates pore boundary separation in MgO-doped alumina at two different pore spacings. In Figure 6a, which corresponds to a pore spacing of 4 μm, pore separation has just initiated after a 2.5 h anneal at 1600°C. In Figure 6b, with a pore spacing of 6 μm, pore separation has just been completed.

Measurements of the migration kinetics included measurements of the pore velocity just prior to pore-boundary separation (*e.g.*, as illustrated in Figure 6a), and thus, measurements of pore velocities approaching the peak pore velocity. When measurements errors are taken into account, peak pore velocities for growth

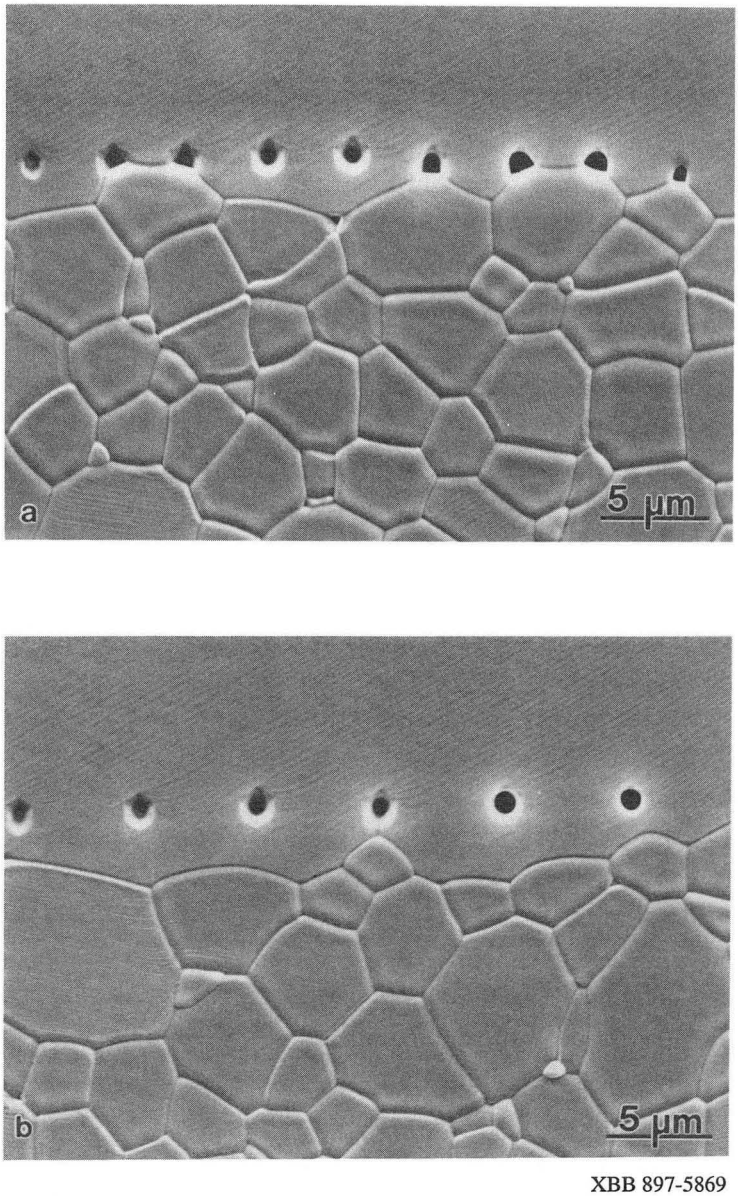

XBB 897-5869

Figure 6 Illustration of effect of pore density on the onset of pore separation during growth of prismatic plane sapphire into MgO-doped alumina at 1600°C. After a 2.5 h anneal, pore separation has (a) just initiated for an interface with a pore spacing of 4 μm, and (b) and has just been completed in a sample with a pore spacing of 6 μm.

into undoped alumina were 0.08-0.22 μm/h for the basal plane seed, and 0.06-0.20 μm/h for the prismatic plane seed. The corresponding values for seed growth into MgO-doped alumina were 0.45-0.70 μm/h and 0.12-0.60 μm/h for basal and prismatic plane sapphire seeds, respectively. Using the analysis by Hsueh *et al.*,[26]

these peak pore velocities can be used to estimate the surface diffusivity. At 1600°C, the surface diffusion coefficient was $\approx 1 \times 10^{-7}$ cm^2/s for undoped alumina and $\approx 4 \times 10^{-7}$ cm^2/s for MgO-doped alumina. The values appeared to be insensitive to the seed orientation for the two seed orientations studied. Thus, at 1600°C, the surface diffusion coefficient in alumina is increased by a factor of between 2 and 10 through the addition of 250 ppm MgO.

The substitution of the peak pore velocities into an expression treating pore-boundary separation in the case of constant center-to-center pore spacing[75] predicts critical grain size pore spacing coordinates at which separation initiates. For the growth of single-crystal sapphire seeds into a dense polycrystalline alumina matrix with an average grain size $\overline{G}$, separation is predicted when

$$\overline{G} < \frac{3f^2}{\pi r}\left(1 - \frac{v_p}{v_b}\right) \tag{21}$$

where f is the center to center pore spacing, r is the (equivalent spherical) pore radius, and v_b is the velocity of a pore-free broundary into the polycrystalline matrix. The critical grain size for separation is therefore proportional to the product of two terms, one dependent upon geometric parameters only, and the other dependent upon kinetic parameters, i.e., the pore velocity/pore-free boundary velocity ratio. As illustrated, f and r can be varied and controlled using lithography. The average grain size $\overline{G}$, the velocity of the pore-free interface v_b, and the peak pore velocity are experimentally measurable. Thus, ***all*** the the relevant parameters can either be controlled or measured. One can therefore predict regions of pore attachment and pore-boundary separation. Since v_b and $\overline{G}$ are interdependent, the critical condition is determined by numerical interation.

The pore size-grain size coordinates predicted by the aforementioned analysis divide a map of grain size and pore spacing into regions of pore separation and pore attachment. In the absence of any measurement errors, a single line would divide such a plot into attachment and separation regions. In practice, the uncertainty due to measurement errors results in a transition region that partitions the plot. A comparison between experimental data and theoretical prediction is provided in Figure 7. The experimental data reflect the behavior of entire pore arrays. Squares are used to designate attachment, and triangles are used to designate separation. The region marked **A** defines combinations of pore spacing and grain size that are predicted to fall within the attachment regime. Similarly, Region **C** corresponds to the conditions yielding separation. The uncertainty in the peak pore velocity broadens the ideal transition line into a transition region which is indicated as Region **B.**

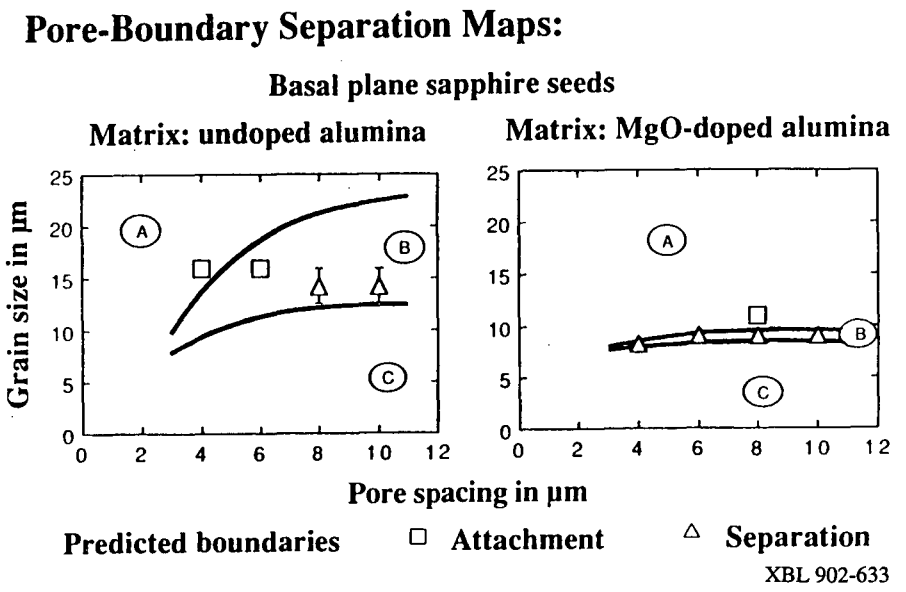

Figure 7 Pore-boundary separation maps for the growth of basal plane sapphire seeds into undoped and MgO-doped alumina at 1600°C.

Two points are noteworthy. First, the experimental results indicate a reduction in the critical grain size (increase in the critical driving force) for separation with the addition of MgO. This leads to an enlargement of the attachment region. Second, the predictions also show this trend, and there is quite good agreement with the experimental observations. In undoped and MgO-doped alumina, the predicted and experimentally observed positions of the pore-boundary separation region agreed to within a few micrometer in grain size. In view of the approximations that were made in the analysis,[26,74] these results are very encouraging.

The opportunities for further research are great. Controlled pore drag experiments have made it possible to measure a surface diffusivity in a model experiment that simulates closely specific microstructural processes of interest, *i.e.*, pore drag and pore-boundary separation. The reproducibility and accuracy of the method provides an opportunity to determine the effect of impurity additions on surface transport on moving interfaces. Clearly, the effects of impurity additions other than MgO to alumina can be tested using the same methodology. Other dopant-matrix combinations can also be investigated. Thus, this technique should prove to have widespread applicability.

4. SUMMARY AND CONCLUSIONS

This paper has focused on the role that interfaces play during sintering of ceramics. Both the energetics and transport properties of solid-vapor, solid-liquid, and solid-solid interfaces play important roles in defining the path of microstrucutral evolution. An effort has been made to highlight some of the more recent contributions to the literature that have brought new theoretical insights to the problem of microstructural evolution in ceramics, or that have provided new tools for studying specific aspects of microstructural evolution with more rigor than had previously been possible. Perhaps the material presented in this paper, in conjunction with the material presented in other contributions to this volume, will stimulate additional modelling efforts and indicate some new as yet unexplored applications of lithography to the study of interfaces in ceramics.

ACKNOWLEDGEMENTS

Many colleagues, too many to list, deserve thanks for sharing their insights on many of the issues discussed in this paper. Discussions with Rowland Cannon over a period of many years have been particularly stimulating. Thanks are due to Jürgen Rödel; his skill and effort made much of the lithography-based research described possible. The past and ongoing lithography research described in this paper was supported by the Director, the Office of Energy Research, Office of Basic Energy Sciences, Materials Sciences Division of the U.S. Department of Energy under Contract No. DE-AC03-76SF00098, and by the National Science Foundation under Contract No. DMR-8821328.

REFERENCES

1. G. W. Scherer, J. Am. Ceram. Soc. 73 (1990) 3-14.

2. J. Lewis and M. Cima, Direct observation of binder distribution processes in 2-D porous networks during thermolysis, in: Ceramic Powder Science III, (Ceramic Transactions, Vol. 12), eds. G. L. Messing, S. Hirano and H. Hausner, (The American Ceramic Society, Westerville, OH, 1990) pp. 583-90.

3. D. W. Sproson and G. L. Messing, Organic binder removal processes in closed pore organic-powder compacts, in: Ceramic Powder Science II, (Ceramic Transactions, Vol. 1), eds. G. L. Messing, E. R. Fuller, Jr., and H. Hausner, (The American Ceramic Society, Westerville, OH, 1988) pp. 528-37.

4. S. J. Glass and D. J. Green, Fabrication of multiphase ceramics by infiltration into powder compacts, in: Ceramic Powder Science IIB, Ceramic Transactions, Vol. 1, eds. G. L. Messing, E. R. Fuller Jr. and H. Hausner, (The American Ceramic Society, Westerville, OH, 1988) pp. 784-91.

5. Maasaki Hama, D. M. Dabbs and I. A. Aksay, Low temperature sintering of ceramic materials, U.S. Patent Application Number 109485.

6. W. B. Hillig, J. Am. Ceram. Soc. 71 (1988) C96-C99.

7. C. Toy and W. D. Scott, J. Am. Ceram. Soc. 73 (1990) 97-101.

8. D. P. Stinton, A. J. Caputo and R. A. Lowden, Am. Ceram. Soc. Bull. 65 (1986) 347-50 .

9. C. H. Herring, J. Appl. Phys. 21 (1950) 301-03 .

10. M. F. Yan, Mat. Sci. and Eng. 48 (1981) 53-72 .

11. R. M. Cannon and W. C. Carter, J. Am. Ceram. Soc. 72 (1989) 1550-54.

12. W. C. Carter and R. M. Cannon, Ceramic Transactions 7 (1990) 137-163.

13. R. J. Brook, Proc. Brit. Ceram. Soc. 32 (1982) 7-24.

14. K. A. Berry and M. P. Harmer, J. Am. Ceram. Soc. 69 (1986) 143-49.

15 N. J. Shaw and R. J. Brook, J. Am. Ceram. Soc. 69 (1986) 107-110.

16. R. L. Coble, J. Am. Ceram. Soc. 56 (1973) 461-66.

17. A. G. Evans, J. Am. Ceram. Soc. 65 (1982) 497-501.

18. W. D. Kingery and B Francois, in: Sintering and Related Phenomena, eds. G. C. Kuczynski, N. Hooton and C. Gibbon, (Gordon and Breach, New York, 1967) pp. 471-79.

19. R. M. Cannon, On the effects of dihedral angle and pressure on the driving forces for pore growth or shrinkage, unpublished research, 1981.

20. F. F. Lange, J. Am. Ceram. Soc. 67 (1984) 83-89.

21. W. C. Carter and A. M. Glaeser, Stability of pores: Effects of dihedral angle distributions, to be submitted to J. Am. Ceram. Soc.

22. C. H. Handwerker and J. Blendell, J. Crystal Growth 75 (1986) 138-60.

23. T. K. Gupta, J. Am. Ceram. Soc. 61 (1978) 191-95.

24. J. Rödel and A. M. Glaeser, J. Am. Ceram. Soc. 70 (1987) C172-C175.

25. J. Rödel, Ph.D. thesis, Department of Materials Science and Mineral Engineering, University of California, Berkeley, October 1988.

26. C. H. Hsueh, A. G. Evans and R. L. Coble, Acta Metall. 30 (1982) 1269-79.

27. C. Handwerker, J. M. Dynys, R. M. Cannon and R. L. Coble, J. Am. Ceram. Soc. 73 (1990) 1365-70.

28. C. Handwerker, J. M. Dynys, R. M. Cannon and R. L. Coble, J. Am. Ceram. Soc. 73 (1990) 1371-77.

29. M. Locatelli and A. M. Glaeser, unpublished research (1991).

30. M. F. Ashby, Scripta Metall. 3 (1969) 837-42.

31. E. Arzt, M. F. Ashby, and R. A. Verrall, Acta Metall. 31 (1983) 1977-89.

32. J. K. McCoy and R. R. Wills, Acta Metall. 35 (1987) 577-85.

33. A. W. Searcy, private communication.

34. J. Rödel and A. M. Glaeser, Materials Letters 6 (1988) 351-355.

35. C. Herring, Phys. Rev. 82 (1951) 87.

36. C. Herring, "The use of classical macroscopic concepts in surface-energy problems, in: Structure and Properties of Solid Surfaces, eds. R. Gomer and C. S. Smith (The University of Chicago Press, Chicago, 1953).

37. J. Rödel and A. M. Glaeser, "Microdesigned interfaces: New opportunities for materials science," *in press*, J. Jap. Ceram. Soc.

38. J. Rödel and A. M. Glaeser, Morphological evolution of pore channels in alumina, in: Sintering of Advanced Ceramics, eds. C. A. Handwerker, J. E. Blendell and W. A. Kaysser (The American Ceramic Society, Columbus, OH, 1990) pp. 243-57.

39. J. Rödel and A. M. Glaeser, J. Am.Ceram.Soc.73 (1990) 592-601.

40. A. Nickles, J. Powers and A. M. Glaeser, unpublished research (1990).

41. S. Baik and C. L. White, J. Am. Ceram. Soc. 70 (1987) 682-88.

42. S. Baik, Surface and grain boundary segregation of Mg and Ca during sintering of alumina, Paper 30-SV-90 presented at 92nd Annual Meeting of the American Ceramic Society, April 22-26, 1990.

43. M. F. Yan, R. M. Cannon, and H. K. Bowen, Grain boundary migration in ceramics, in: Ceramic Microstructures '76, eds. R. M. Fulrath, and J. A. Pask (Westview Press, Boulder, Colorado 1977) pp. 276-307.

44. D. Turnbull, Trans. A.I.M.E. 191 (1951) 661-65.

45. J. W. Cahn, Acta Metall. 10 (1962) 789-98.

46. a) K. Lücke and H. P. Stüwe, On the theory of grain boundary motion, in: Recovery and Recrystallization of Metals (Gordon and Breach 1963) pp. 171-210. b) K. Lücke and H. P. Stüwe, Acta Metall.19 (1971) 1087-99.

47. a) M. F. Yan, R. M. Cannon and H. K. Bowen, J. Appl. Phys. 54 (1983) 764-78. b) M. F. Yan, R. M. Cannon and H. K. Bowen, ibid (1983) 779-791.

48. P. G. Shewmon, Trans. A.I.M.E. 230 (1964) 1134-37.

49. F. F. Nichols, J. Appl. Phys. 37 (1966) 4599.

50. R. J. Brook, Controlled grain growth, in: Treatise on Materials Science and Technology, Vol. 9, ed. F. F. Y. Wang (Academic Press, New York, 1976) pp. 331-64.

51. R. J. Brook, J. Am. Ceram. Soc. 52 (1969) 56-57.

52. H. G. Müller, Z. Phys. 96 (1935) 279-306.

53. M. F. Yan, Grain boundary mobility of KCl Sc.D. thesis, Massachusetts Institute of Technology (1976).

54. a) A. M. Glaeser, H. K. Bowen and R. M. Cannon, J. Am. Ceram. Soc. 69 (1986) 119-26. b) A. M. Glaeser, H. K. Bowen and R. M. Cannon, ibid, 299-309.

55. R. C. Sun and C. L. Bauer, Acta Metall. 18 (1970) 635-38.

56. D. W. Demianczuk and K. T. Aust, Acta Metall. 23 (1975) 1149-62

57. R. Viswanathan and C. L. Bauer, Acta Metall. 21 (1973) 1099-1109.

58. R. C. Sun and C. L. Bauer, Acta Metall. 18 (1970) 639-47.

59. K. Kitazawa, T. Arima, N. Bessho, Y. Saito, K. Fueki and T. Mukaibo, Sci. of Sintering 10 (1978) 27-33.

60. R. L. Coble and J. E. Burke, Sintering of ceramics, in: Progress in Ceramic Science,Vol. 3, ed. J. E. Burke (Pergamon Press, London, 1963) pp. 197-251.

61. R. D. Monahan and J. W. Halloran, J. Am. Ceram. Soc. 62 (1979) 564-567.

62. M. Kinoshita, Yogyo-Kyokai-Shi 82 (1974) 295-296.

63. W. A. Kaysser, M. Sprissler, C. A. Handwerker and J. E. Blendell, J. Am. Ceram. Soc. 70 (1987) 339-343.

64. Y. Finkelstein, S. M. Wiederhorn, B. J. Hockey, J. E. Blendell and C. A. Handwerker, Migration of sapphire into vitreous bonded aluminum oxide, in: Sintering of Advanced Ceramics, eds. C. A. Handwerker, J. E. Blendell and W. A. Kaysser (The American Ceramic Society, OH, 1990) pp. 258-279.

65. S. J. Bennison and M. P. Harmer, J. Am. Ceram. Soc. 66 (1983) C- 90-C-92.

66. S. J. Bennison and M. P. Harmer, J. Am. Ceram. Soc. 68 (1985) C-22-C-24.

67. Y. M. Chiang and W. D. Kingery, J. Am. Ceram. Soc. 72 (1990) 271-78

68. S. L. Hwang and I. W. Chen, J. Am. Ceram. Soc. 73 (1990) 3269-77.

69. K. T. Aust and J. W. Rutter, Grain boundary migration, in: Recovery and Recrystallization of Metals, ed. L. Himmel (Gordon and Breach, NY, 1963) pp. 131-169.

70. J. Rödel and A. M. Glaeser, J. Am. Ceram. Soc. 73 (1990) 3293-301.

71. C. A. Handwerker, R. M. Cannon and R. L. Coble, Final-stage sintering of MgO, in: Advances in Ceramics, Vol. 10, Structure and Properties of MgO and Al_2O_3 Ceramics, ed. W. D. Kingery (American Ceramic Society, Columbus, OH, 1984) pp. 619-43.

72. M. Sakarcan, C. H. Hsueh and A. G. Evans, J. Am. Ceram. Soc. 66 (1983) 456-61.

73. J. Rödel and A. M. Glaeser, Pore drag in alumina, in: Sintering of Advanced Ceramics, eds. C. A. Handwerker, J. E. Blendell and W. A. Kaysser (The American Ceramic Society, Columbus, OH, 1990) pp. 280-95.

74. J. Rödel and A. M. Glaeser, J. Am. Ceram. Soc. 73 (1990) 3302-12.

75. F. M. A. Carpay, J. Am. Ceram. Soc. 60 (1977) 82-83.

LAWRENCE BERKELEY LABORATORY
UNIVERSITY OF CALIFORNIA
INFORMATION RESOURCES DEPARTMENT
BERKELEY, CALIFORNIA 94720